Feature article

Block copolymer template-directed synthesis of well-ordered metallic nanostructures

Ivana Vukovic, Gerrit ten Brinke*, Katja Loos*

Department of Polymer Chemistry, Zernike Institute for Advanced Materials, University of Groningen, Nijenborgh 4, 9747 AG Groningen, The Netherlands

ARTICLE INFO

ABSTRACT

3D nanostructured inorganic materials appear as promising candidates for various practical applications. Here we focus on metal nanofoams, a class of 3D nanomaterials uniquely combining the properties of metals and nanoporous materials, and review the recent developments in their preparation methods. Common approaches, such as dealloying, sol–gel synthesis, nanosmelting, combustion synthesis, etc., render metallic nanostructures with highly disordered architectures which might have adverse effects on their mechanical properties. In contrast, block copolymers have the ability to self-assemble into bicontinuous ordered nanostructures that can be applied as templates for the preparation of well-ordered metal nanofoams. Several examples of block copolymer template-directed synthesis of continuous metallic nanostructures will be described and the prospects of this approach will be discussed.

© 2013 Elsevier Ltd. All rights reserved.

1. Introduction

To fulfill the constant quest for novel functional materials, the cooperation and development of research areas, such as material science, chemistry, physics, and biology, is required. Nowadays, much attention is given to the field of nanostructured materials that, by definition, have at least one dimension in the range from 1 to 100 nm. In comparison to macroscopic systems, nanomaterials have advanced properties arising from their nanoscale dimensions. Zero-dimensional (0D) nanostructures, nanoparticles, are widely applied in biology and medicine for probing of DNA structure [1], MRI contrast enhancement [2], tissue engineering [3,4], cancer therapy [5], etc. Furthermore, they find application in food packaging and food safety [6], as catalysts with enhanced performance [7], for hydrogen storage [8,9], data storage [10], etc. One-dimensional (1D) nanostructures (e.g., wires, rods, tubes) are expected to play an important role as both interconnects and functional units in fabricating electronic, optoelectronic, electrochemical, and electromechanical nanodevices [11,12]. Several methods have been used to fabricate 1D nanostructures including template-directed synthesis, self-assembly of 0D nanostructures, size reduction of 1D microstructures, electrospinning and others. For example, Park et al.

demonstrated the preparation of metallic line patterns using functional block copolymer templates [13]. Polystyrene-*block*-poly(2-vinylpyridine) (PS-*b*-P2VP) and poly(2-vinylpyridine)-*block*-poly(-methyl methacrylate) (P2VP-*b*-PMMA) block copolymers were spin-coated onto Ag-coated silicon substrate and annealed under solvent vapor to achieve the desired surface morphology. Subsequently, porous block copolymers were obtained by either reconstruction of the P2VP block in ethanol or removal of the PMMA block by UV irradiation followed by rinsing with acetic acid. Finally, silver line patterns were generated using electrochemical etching or direct metal evaporation and lift-off processes. 2D nanostructures, like thin films, can be grown by vapor-phase (sputtering, chemical vapor deposition, atomic layer deposition, etc.) or liquid-phase deposition (electrochemical deposition, Langmuir–Blodgett films, self-assembled monolayers, etc.) [14–16]. Finally, 3D nanostructures represent the ultimate form factor for a number of materials. However, their creation is a rather delicate task [17]. The available top-down approaches are extremely challenging: lithography techniques allow precise patterning, but can only be implemented in an inherently 2D manner, whilst the available 3D microscale techniques cannot be easily translated to the nanoscale. Currently, the attention is focused on bottom-up approaches that are usually based on self-assembling processes often similar to those occurring in nature.

In this feature article we discuss 3D nanostructured metals. First, we describe the established methods for metal nanofoam preparation and their limitations in terms of ordering at the

* Corresponding authors.
  E-mail addresses: g.ten.brinke@rug.nl (G.ten Brinke), k.u.loos@rug.nl, katjaloos@web.de (K. Loos).

nanoscale. Then, we discuss the application of block copolymers and block copolymer based systems as precursors to metallic nanostructures and suggest the possibilities to overcome the aforementioned limitations with examples of block copolymer template-directed synthesis of metal nanofoams. Finally, we end with a brief outlook on the future trends in this research area.

2. Metal nanofoams: properties and preparation methods

A nanoporous metal foam is defined as a three-dimensional structure comprised of interconnected metallic features with a porosity greater than 50 vol% and in which sub-micron pores significantly contribute to the specific surface area of the foam [18]. Metal nanofoams have, on the one hand, properties characteristic of metals such as electrical and thermal conductivity, catalytic activity and ductility/malleability whilst, on the other hand, also display properties characteristic of nanostructured materials such as high surface area, ultralow density and high strength-to-weight ratio. Due to this unique combination, metal nanofoams appear as candidates for a number of technological applications. Several examples are described in the following paragraph.

Hydrogen is an environmentally friendly energy carrier and its storage is one of the key challenges in the hydrogen economy. It can be stored as pressurized gas, cryogenic liquid or solid fuel as a combination with other materials such as metal hydrides. Due to safety reasons, metal hydrides are the preferable option for hydrogen storage and it has been demonstrated that in comparison to bulk material, nanostructured metals significantly improve the reaction kinetics, reduce the enthalpy of metal hydrides formation, lower the hydrogen absorption and release temperatures [19–21]. Nanoporous metals and their derivates can also be employed for the production of novel 3D-structured batteries. Open porous networks and thin ligaments enable fast diffusion of ions into and out of electrodes, thus, creating fast discharging and recharging batteries [22]. Due to the size-effect-enhanced catalytic properties, nanostructured metals, such as nickel, could be a low-cost substitution for precious-metal catalysts [18]. Furthermore, literature reports the tunability of the physical properties of nanoporous metals through an applied voltage [23,24]. Injection of the surface charges into a porous metal nanofoam enhances the surface stresses leading to its expansion or contraction. Actuation properties of metallic nanofoams have been proven experimentally [25]. A bilayer foil consisting of solid and nanoporous gold layer was immersed in aqueous electrolyte and the electrochemical potential varied. The nanoporous layer expanded or shrunk whilst the solid one maintained its original dimensions, and thus, the bilayer foil bent with a tip displacement of several millimeters. The observed strain was orders of magnitude larger than in conventional cantilever bending experiments. Metal nanofoams can also be applied as implant materials as they have a high strength-to-weight ratio and assist osseointegration. The high porosity and interconnected nanochannels enhance bone ingrowth and insure the long-term stability of the implant [26,27].

Several approaches for the preparation of nanoporous metal foams have been established. Erlebacher et al. reported the formation of nanoporous gold by the dealloying process from a binary alloy of silver and gold [28]. Silver, as a less-noble metal, can be etched away either electrochemically or by using acid, resulting in a nanoporous gold network with a ligament spacing of *ca.* 10 nm (Fig. 1). The morphology of nanoporous gold in terms of sizes of ligaments and pores can be controlled by varying the dealloying potential [29]. An interesting approach in which the dealloying is combined with templating to render hierarchically porous gold has been reported by Nyce et al. [30] First, Ag–Au alloy was electroless plated onto micron-sized spheres of polystyrene and then the
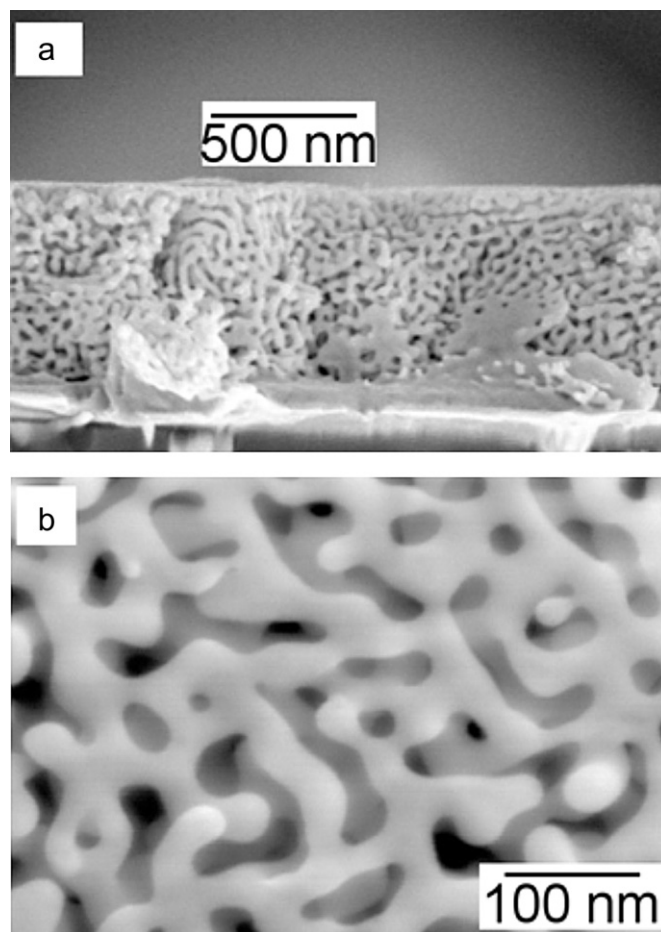

Fig. 1. Scanning electron micrographs of nanoporous gold obtained from Ag–Au alloy by selective Ag etching in nitric acid: (a) Cross-section of dealloyed $Ag_{32\%}Au_{68\%}$, (b) Plan view of dealloyed $Ag_{26\%}Au_{74\%}$ (atom%). Adapted from Ref. [28].

polymer was removed by pyrolysis. Finally, silver was etched away from Ag–Au alloy using nitric acid leaving behind hierarchically porous gold.

Sol–gel techniques are well-developed for the synthesis of metal nanoparticles, but their applicability to assemble nanoparticles into metal foams appears to be very challenging. It has
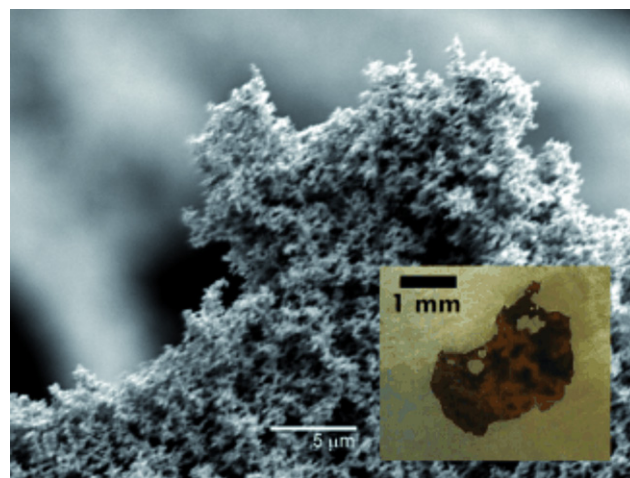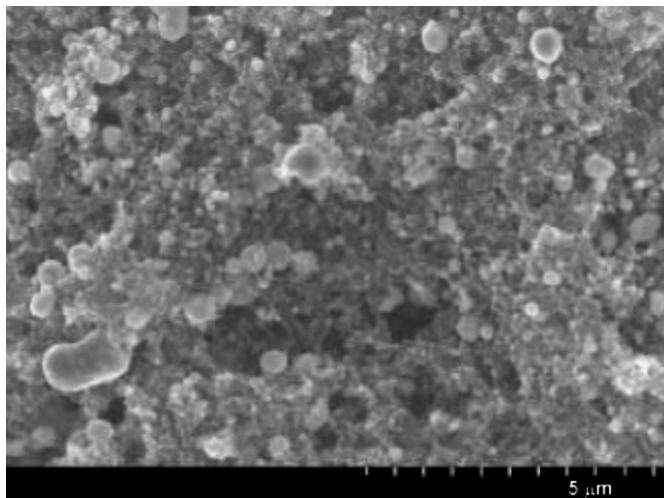

Fig. 2. Scanning electron micrograph of nanoporous gold obtained from sol–gel approach. Reprinted from Ref. [18].

Fig. 3. Scanning electron micrograph of iron aerogel prepared by nanosmelting of RF/iron oxide aerogel. Reprinted from Ref. [18].

been found that the solubility of metal nanoparticles and the removal of the stabilizing ligand are the most important criteria for successful preparation of porous metals [31]. In one example of gold nanofoam preparation via the sol−gel route, highly water-soluble Au nanoparticles (solubility up to 30 wt%), stabilized with a mixture of hydrophilic and hydrophobic ligands, were dissolved in water and the solution was oxidized with hydrogen peroxide. Nanostructured gold precipitates were formed after 48 h (Fig. 2) [18].

Leventis et al. have recently reported a viable route towards metal nanofoams through nanosmelting of hybrid polymer/metal aerogels [32]. Using the sol−gel approach, an aerogel consisting of resorcinol-formaldehyde (RF) polymer and iron oxide was prepared. Subsequently, the aerogel was exposed to high temperatures

Fig. 4. Schematic representations of block copolymer structures showing only the domains of the minority phase. The lamellar (LAM), cylindrical (CYL) and the spherical (SPH) morphology are three examples of common, classical phases and the gyroid (GYR), perforated lamellar (PL), and the ordered bicontinuous double diamond (OBDD) are three examples of the more complex morphologies revealed in diblock copolymers. The enlarged view of the LAM phase depicts the self-assembly of individual block copolymer chains within this morphology. Reprinted with permission from Ref. [42].

(800−1000 °C) under argon atmosphere, which led to simultaneous polymer degradation and iron oxide reduction to metallic iron (Fig. 3). Similarly, the preparation of porous Cu, Ni, Sn, and Co networks by nanosmelting has been demonstrated [33].
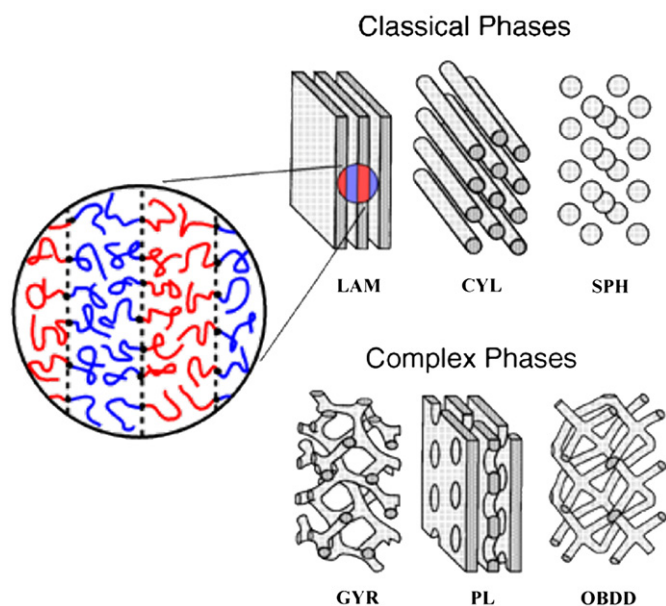
Combustion synthesis represents another pathway for the nanostructured metal production, in which metal is mixed with the energetic precursor that releases energy during its decomposition and drives the formation of metal nanofoam. Tappan et al. have demonstrated the preparation of nanoporous Fe, Cu, Co, and Ag via combustion synthesis [34].

As described, utilizing previously presented techniques, one can prepare highly porous metal foams with nano-sized pores. However, the prepared foams are typically highly disordered which disables the effective stress transmission from the ligament nanoscale to the overall macroscale and results in poor mechanical properties [35−37]. The ordering issue can be overcome in the alternative block copolymer template-directed approach for metal nanofoam synthesis.

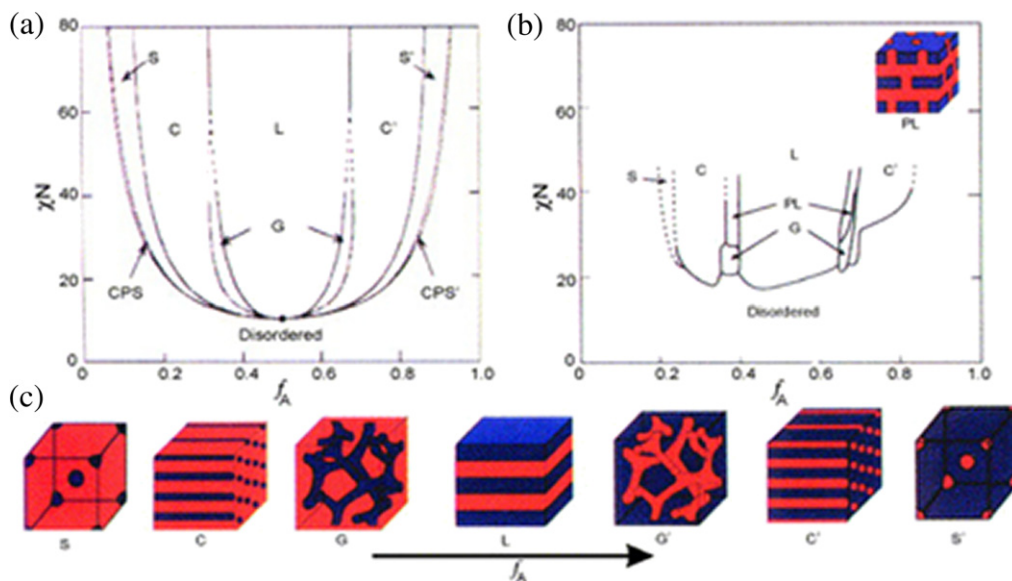## 3. Self-assembled block copolymers and supramolecular complexes

Chemically distinct polymers generally do not mix, but macrophase separate, in a similar fashion to oil and water. In a block copolymer, two or more chemically different homopolymers are covalently linked and this linkage prevents macrophase separation. However, due to the unfavorable interactions between the different blocks, phase separation still occurs but, because of their connectivity, only on the nanometer scale and this process is called microphase separation. The unfavorable interactions between chemically distinct species induce stretching of the polymer chains (*i.e.*, to minimize the interaction enthalpy) and the entropic elasticity (of the entropic spring) resists this stretching (*i.e.*, to maximize the conformational entropy). This enthalpy-entropy balance governs the microphase separation in block copolymers. Experimentally, the block copolymer phase behavior can be controlled by the selection of the composition and the architecture of the block copolymer, the overall degree of polymerization and the segment−segment interaction parameter [38−41]. The schematic illustrations of the most common, classical and some complex phases are depicted in Fig. 4, illustrating the domains of the minority phase. In the enlarged view of the lamellar morphology, the self-assembly of individual molecules within the domains is shown where blue and red parts represent the two chemically distinct blocks [42]. The phase diagram of diblock copolymers was theoretically predicted using self-consistent mean-field theory (Fig. 5a) [43,44]. Experimental phase diagrams are found to generally be similar to the calculated one, except that they appear more asymmetric. The experimentally determined phase diagram of polystyrene-*block*-polyisoprene (PS-*b*-PI) is represented in Fig. 5b [45,46]. As the number of blocks in the copolymer increases, possibilities for novel, complex structures are created. Several examples include three-domain lamellae, core−shell or alternating spheres, cylinders, and gyroid, perforated structures and others [46−50]. Similarly, complex polymer architectures give rise to new, intriguing morphologies. For instance, a star-shaped architecture results in Archimedean tiling pattern morphologies that are unique for this type of copolymer [51].

When additional components are combined with copolymer systems, the obtained complexes exhibit interesting phase behavior. Supramolecular complexes are defined as assemblies of molecules held together by non-covalent interactions. A specific example of a supramolecular complex is the so-called comb-coil block copolymer in which one of the blocks, namely the comb block, contains side chains that are non-covalently linked to the

Fig. 5. (a) Block copolymer phase diagram as calculated using the self-consistent mean-field theory, (b) Experimentally determined phase diagram of PS-*b*-PI. Schematic representations of different morphologies are given below. Reprinted with permission from Ref. [46]. Copyright 1999, American Institute of Physics.

main chain, usually via hydrogen bonds. A supramolecular complex of polystyrene-*block*-poly(4-vinylpyridine) (PS-*b*-P4VP) and pentadecylphenol (PDP) has been extensively studied in the group of Ikkala and our group [52–55]. Each PDP molecule contains a hydroxyl group which can act as a hydrogen-bond promoting group and each repeating unit of P4VP contains a nitrogen atom that can act as a hydrogen-bond accepting group. Therefore, if PDP is added to P4VP, hydrogen bonds are formed between the nitrogen of the pyridine ring and the hydrogen on the phenol ring. The chemical structure and the schematic representation of the PS-*b*-P4VP(PDP) supramolecule is illustrated in Fig. 6a. Non-polar PDP alkyl tails microphase separate from P4VP in such a way that PDP molecules align perpendicularly to the P4VP homopolymer which gives rise to the formation of two length scale structures-within-structures (Fig. 6b). The variation in the PDP content allows for the simple tuning of the long-length scale morphology of the complex [56–58]. Furthermore, PDP can be selectively removed by an appropriate solvent (*e.g.*, ethanol) resulting in nanoporous polymer material [59,60].

4. What do block copolymers and butterflies have in common?

The gyroid morphology was first identified in 1967 in strontium soaps by Luzzatti and Spegt [61]. Three years later, this bicontinuous triple periodic minimal surface was mathematically described by the NASA physicist Alan Schoen and named "gyroid" [62]. The single gyroid contains the percolated network and matrix phases and it is characterized by the $I4_132$ symmetry, whilst the double gyroid with $Ia\bar{3}d$ symmetry has two parallel network phases that are related by inversion (Fig. 7) [63]. The transmission electron micrographs typical for a bicontinuous polymer phase were published already in 1976, but the authors did not comment on the bicontinuous nature of the system [64]. The bicontinuous ordered polymer structure was reported for the first time in 1986 by Alward et al. in a star-block copolymer comprised of PS-*b*-PI arms [65]. Thomas et al. described the observed morphology as the ordered bicontinuous double diamond (OBDD) with $Pn3m$ symmetry [66]. However, theoretical calculations that followed did not provide the evidence that the OBDD is an equilibrium structure in AB diblock copolymers [67–70]. The gyroid morphology in block copolymers has been described for the first time in 1994 [71,72]. Hajduk et al. analyzed a linear diblock copolymer PS-*b*-PI containing 37 wt% PS, using small angle X-ray scattering (SAXS) and transmission electron microscopy (TEM). TEM images suggested the bicontinuous morphology, but SAXS data were inconsistent with the OBDD structure. Peaks in the SAXS pattern were found at the positions $\sqrt{6}$, $\sqrt{8}$, $\sqrt{20}$, $\sqrt{22}$, $\sqrt{32}$ and $\sqrt{38}$ which are allowed by twelve cubic space groups. One of them, the $Ia\bar{3}d$ space group, has additional five allowed reflections that were
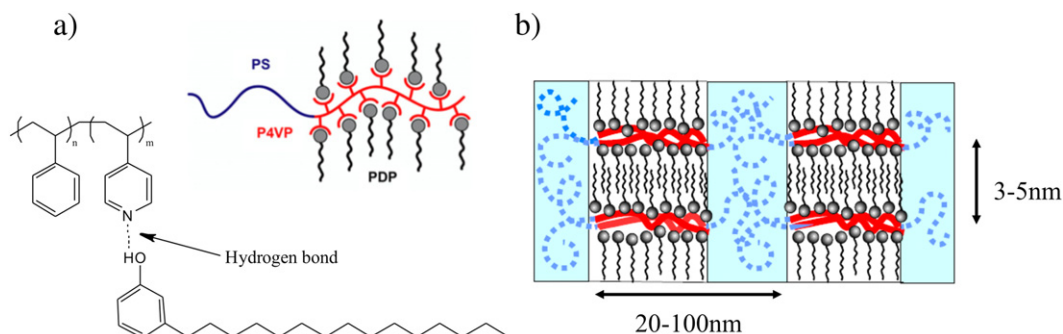
Fig. 6. (a) The chemical structure and the schematic representation of PS-*b*-P4VP(PDP) supramolecule, (b) PS-*b*-P4VP(PDP) supramolecules self-assemble into hierarchically ordered structures-within-structures.
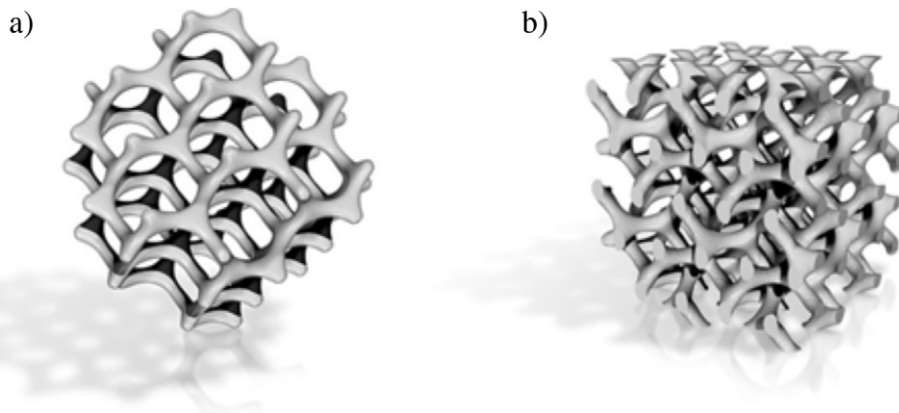
Fig. 7. (a) The single gyroid morphology with $I4_132$ symmetry, (b) the double gyroid morphology with $Ia\bar{3}d$ symmetry. Adapted with permission from Ref. [116].

not present in the experimental Bragg pattern, whilst the others have seven or more. A space filling model with $Ia\bar{3}d$ symmetry was generated and used to predict SAXS and TEM results. They found a good agreement between the predicted and the experimental data [71]. Theoretical calculations that followed confirmed that the double gyroid can be an equilibrium structure in AB diblock copolymers [43]. In more complicated block copolymer systems, such as block copolymer blends, variations of double gyroid morphology have been discovered. The core–shell double gyroid phase is one example in which gyroid networks are built out of two different polymer blocks, one being a core and the other a corona of gyroid networks that are embedded in the third polymer block that represents a gyroid matrix [73].

The double gyroid as an isotropic structure with continuous triple periodic percolated domains appears to be superior to classical morphologies (lamellar, cylindrical or spherical) for a number of technological applications. For instance, the gyroid structure, due to the high interfacial area per specimen volume, could be exploited for gas separation purposes [74]. Shefelbine et al. prepared ABC triblock copolymer with the core–shell double gyroid morphology. Glassy polystyrene was chosen as a middle block that separated two rubbery end blocks − polyisoprene and polydimethylsiloxane. A gas mixture would enter one rubbery block, characterized by high permeability and low selectivity. Further, it would diffuse selectively through a glassy layer and would, finally, be collected from the second rubbery layer. Furthermore, due to the ordering and periodicity in three dimensions, the gyroid structure is an excellent candidate for photonic crystal applications [75–77]. Urbas et al. [76] examined the optical properties of the gyroid forming PS-*b*-PI block copolymer with spacing comparable to the wavelength of visible light. Furthermore, the gyroid forming block copolymers could be used for templating purposes: one block could be selectively removed which results in a porous gyroid template that can be, for example, backfilled with an inorganic material. This will be further elaborated in Section 5 and supported with examples in Section 6. For templating purposes, the gyroid is preferable over anisotropic block copolymer phases (*e.g.*, cylindrical) which often require laborious alignment procedures prior to the application [78–80].

The gyroid structure appears also in nature, namely in butterfly wing scales, and it is responsible for the shimmering wing colors of several butterfly species. Saranathan et al. [81] investigated 3D
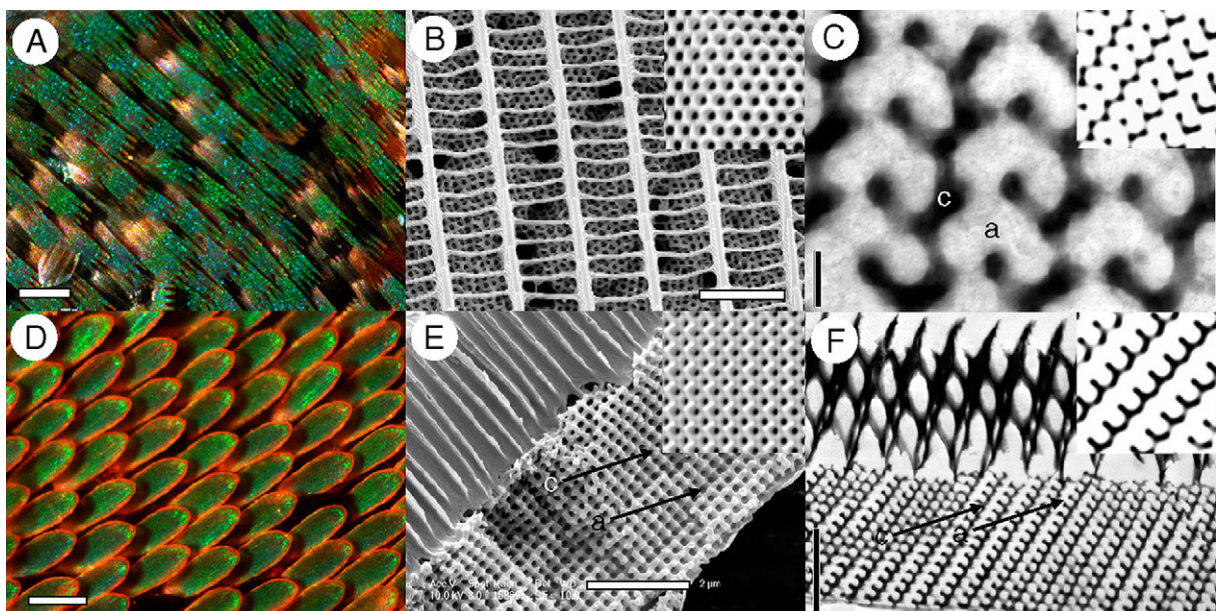
Fig. 8. Anatomy of the structural color-producing nanostructures in lycaenid and papilionid butterflies: (A, D) light micrographs (scale bars 100 μm), (B, E) SEM images (scale bars 2.5 and 2 μm, respectively), (C, F) TEM images (scale bars 200 nm and 2 μm, respectively). Reprinted with permission from Ref. [81].
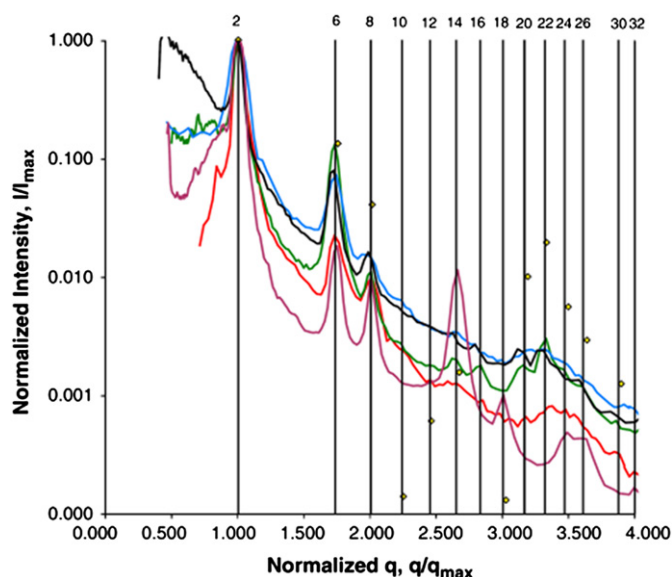
Fig. 9. SAXS patterns of the nanostructures of five different butterfly species indicating the single gyroid morphology with $I4_132$ symmetry. Reprinted with permission from Ref. [81].

photonic nanostructures in five butterfly species by SAXS, TEM and SEM and identified their morphology as the single gyroid with $I4_132$ symmetry (Figs. 8 and 9). The butterflies initially develop the thermodynamically favorable double gyroid phase that consists of two networks, different in composition, embedded in a matrix. Chitin is then deposited on one of the two networks and after the cell dies, the chitin-air structure is left behind. The morphology of the porous chitin structure is single gyroid which is optically more efficient than the double gyroid one. This structure could be mimicked in gyroid forming ABC terpolymers, with two chemically distinct networks [82]. A single gyroid template could be provided by the selective removal of one of the networks.

5. Block copolymer template directed preparation of metal nanofoams

The nanoscale ordering in block copolymer structures can be extended to inorganic materials with more appealing properties, *e.g.*, metals. This process generally encompasses several steps (Fig. 10):

1. Selective removal of the sacrificial polymer block,
2. Backfilling of the porous structure with inorganic material (*e.g.*, metal),
3. Removal of the remaining polymer template.

The first two steps can be combined into one by selective inclusion of inorganic compounds, *e.g.*, metal ions, in one of the copolymer blocks [83].
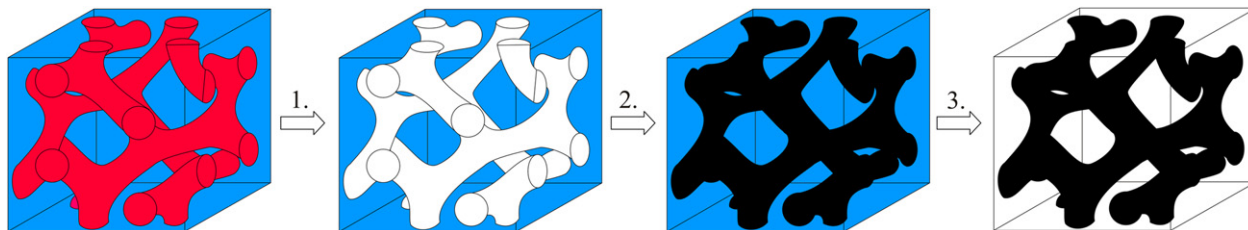
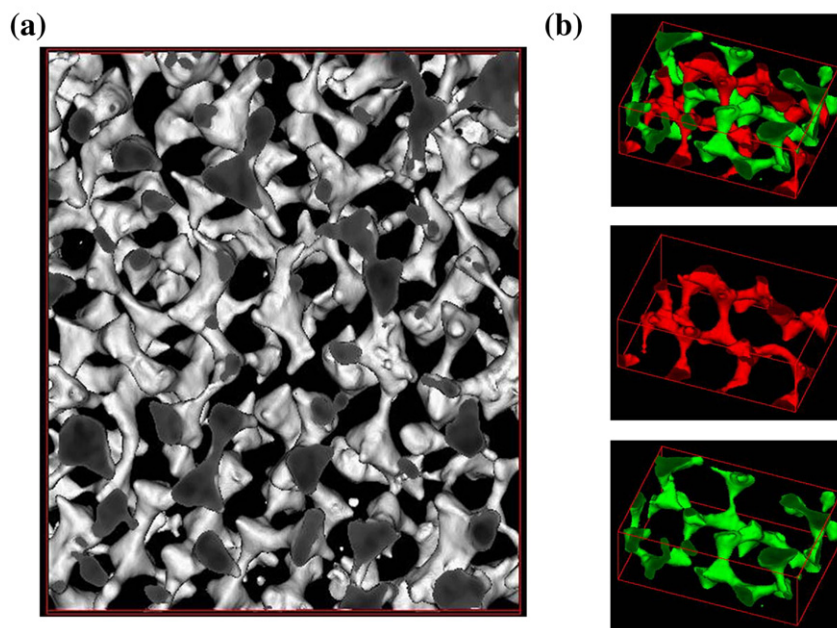### 5.1. Selective removal of the sacrificial polymer block

In recent years, many studies successfully demonstrated the selective degradation of polymer blocks from a self-assembled block copolymer structure. Polydiene blocks, such as polyisoprene (PI) or polybutadiene (PBD), can be etched away via ozonolysis [84–86]. Chen et al. [86] examined the ozonolysis efficiency in blends of block copolymer PS-*b*-PI and homopolymer PS and found a strong dependence on the morphology of the PI microdomains. The degree of ozonization after 24 h reaction demonstrated a decreasing trend from 90, 80, 70 to 50% if the PI microdomains transformed from lamellae, to gyroid network, to cylinders, to spheres, respectively, in the PS matrix, which was attributed to the decrease of the contact area PI/ozone and the accessible volume of PI microdomains.

UV irradiation can be employed for selective removal of PMMA blocks. The exposure of PS-*b*-PMMA block copolymer to UV light leads to degradation of the PMMA phase and simultaneous cross-linking of the PS phase [87]. If a blend of block copolymer PS-*b*-PMMA and homopolymer PMMA is used as a precursor, the nanoporous structure can be generated in two ways: (1) all PMMA (PMMA block and PMMA homopolymer) can be removed by UV irradiation or (2) only PMMA homopolymer can be removed using a selective solvent, namely acetic acid [88].

Polylactic acid (PLA) blocks can be readily removed from a block copolymer (*e.g.*, PS-*b*-PLA) by a mild aqueous base [89–91]. From crystalline-amorphous block copolymers, such as polyethylene-*block*-polystyrene (PE-*b*-PS) or polystyrene-*block*-poly(vinylidene fluoride)-*block*-polystyrene (PS-*b*-PVDF-*b*-PS), the amorphous component can be selectively etched with fuming nitric acid [92,93]. Reactive ion etching can be used to generate porous structures from block copolymer precursors with one etch-resistant block [94–97]. Finally, amphiphilic molecule PDP can be removed from a supramolecular complex containing P4VP(PDP) comb-block by selective dissolution in ethanol, as already mentioned in Section 3, resulting in porous polymer template [54,59,60].

5.2. Backfilling of the porous structure with inorganic material

Metal oxides (*e.g.*, SiO_2 or TiO_2) can be introduced inside the pores of a polymer template via the sol–gel process. In the sol–gel process, the starting colloidal solution − sol, typically composed of metal alkoxides or metal salts, fills pores of a polymer template and subsequently, via hydrolysis and polycondensation reactions, transforms into gel − an integrated network composed of discrete colloidal particles or polymer networks [98]. Hsueh et al. prepared a polystyrene-*block*-poly(L-lactide) (PS-*b*-PLLA) block copolymer with double gyroid morphology and then selectively removed the PLLA block via hydrolysis [99,100]. The obtained porous PS network was filled with amorphous SiO_2 via the sol–gel process. The SAXS pattern, TEM and electron tomography (Fig. 11a) images of the PS/SiO_2 nanohybrid confirmed its double gyroid morphology. After the polymer removal, a gyroid forming SiO_2 network was exposed (Fig. 11b) and its porosity was calculated from nitrogen adsorption

Fig. 10. Block copolymer template directed preparation of ordered inorganic nanostructures: 1. selective removal of the sacrificial polymer block, 2. backfilling of the porous structure with inorganic material (*e.g.*, metal), 3. removal of the remaining polymer template.

(a)   **(b)**

Fig. 11. The reconstructed 3D images of: (a) gyroid PS/SiO$_2$ nanohybrid, (b) gyroid SiO$_2$ composed of two parallel networks related by inversion (red and green). Reprinted with permission from Ref. [99]. Copyright 2010 American Chemical Society.

measurements to be 66%. The refractive index of dense amorphous SiO$_2$ is rather low and it further decreases in the porous sample. The refractive index of the prepared gyroid SiO$_2$ network was estimated to be about 1.1, thus it appeared suitable for optical applications such as antireflection structures [99]. The hydrolysis reaction rate in the sol−gel process towards SiO$_2$ is exceptionally low which allows for complete diffusion of sol into the template pores before the gelation starts. On the other hand, titanium alkoxides are not as stable and pores will be blocked by gel before sol completely penetrates the template. Therefore, to fabricate the gyroid PS/TiO$_2$ nanohybrid, one has to carefully control the reaction conditions. A thermal treatment was employed to remove PS and expose the free-standing, gyroid anatase TiO$_2$ (Fig. 12). Its photocatalytic efficiency was determined by evaluating the degradation of methylene blue under UV irradiation. It was found that the decomposition rate is about two times higher in comparison to commercial TiO$_2$ powder [100].

Electrochemical and electroless plating are commonly used techniques to deposit metals onto or into templates [101−104]. To electrochemically deposit metal inside the pores of a polymer template, the working electrode is usually coated by a template and, together with the counter and the reference electrode, placed in the plating bath and connected to an external source of current. To completely plate the sample, the surface of the underlying working electrode should be accessible to the plating bath, which may appear difficult for thicker polymer templates with many defects or highly complex structure. Also relatively simple polymer templates, such as the cylindrical one, require proper alignment prior to electrochemical plating. In electroless plating, a polymer template is immersed into the electroless plating bath and metal is deposited via an autocatalytic process onto the surface of the template. Electroless plating does not require an external current source and allows plating onto complex shapes and through pores. Furthermore, nonconductive surfaces, such as polymers or ceramics, can undergo electroless plating after the appropriate treatment. The pretreatment usually consists of two steps: (1) sensitization in SnCl$_2$/HCl, when Sn^{2+} ions adsorb onto the template surface, (2) activation in PdCl$_2$/HCl, when Pd sites are formed through the following redox reaction:

Sn^{2+} + Pd^{2+} → Sn^{4+} + Pd^0. The Pd sites act as catalysts during the electroless metal plating procedure. In electroless deposition, metal ions, M^{z+}, are reduced by the reducing agent, R^{n-}, and the process can be simply described as: M^{z+} + R^{n-} → M^0 + R^{z-n}. The process is autocatalytic, *i.e.*, it is catalyzed by metal being deposited. Besides the source of metal ions and the reducing agent, the electroless plating bath usually contains the complexing agent, that acts as a buffer and reduces the concentration of free metal ions, and the stabilizer, that prevents the decomposition of the plating solution.

5.3. Removal of the remaining polymer template

There are several methods to remove polymer from the polymer/inorganic nanohybrid, such as pyrolysis [30,60], dissolution [105,106], UV degradation [99,100], *etc.*

Pyrolysis involves the decomposition of polymer at elevated temperature, leaving behind an inorganic material with preserved morphology. Inorganic materials may as well undergo changes at elevated temperatures. For instance, thermal treatment will increase the crystallinity of TiO$_2$, thus, amorphous TiO$_2$ may transform to one of its crystalline forms: rutile, anatase, and brookite [100]. Another example is nanoporous gold that undergoes thermal coarsening due to the recrystallization in solid state at elevated temperatures [107]. Therefore, the applicability of pyrolysis for polymer template removal depends on the type of inorganic material and its purposes.

6. Examples of metal nanofoams prepared by block copolymer templating

There have been a few reports in the literature demonstrating the replication of complex block copolymer structures into the ordered metal phase. In the following paragraphs, we describe several prominent examples and focus on the fabrication of gyroid metal nanofoams.

Crossland et al. [105] investigated the thin film morphology of poly(4-fluorostyrene)-*block*-poly(D,L-lactide) (PFS-*b*-PLA) that in
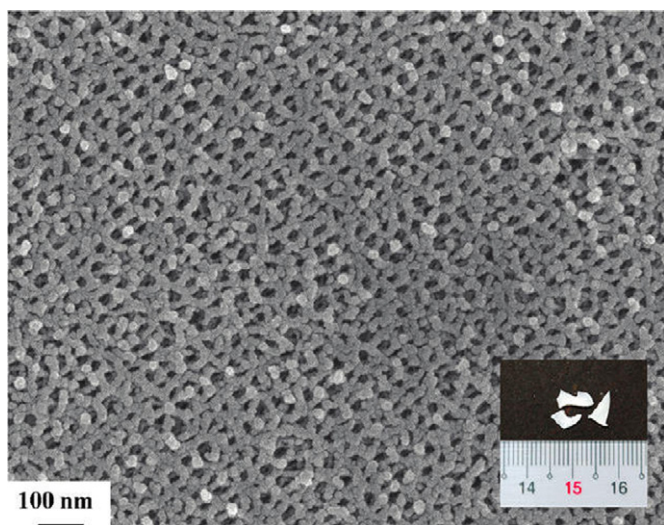
Fig. 12. SEM micrograph of the gyroid anatase TiO_2 network. The inset represents the centimeter-sized bulk sample. Reprinted with permission from Ref. [100]. Copyright 2012 American Chemical Society.

bulk acquires the cylindrical morphology at 150 °C and the gyroid morphology at 180 °C. When the thin film was annealed for 35 h at 180 °C and then cooled down to room temperature over 3 h, it was found to adopt the gyroid phase in the entire sample volume. The PLA block was then selectively removed by hydrolysis in a mild aqueous base and platinum was deposited into the remaining pores via electrochemical deposition. Final removal of the PFS block, by dissolution in toluene or exposure to O_2 plasma, resulted in isolated mounds or a continuous freestanding array of a gyroid Pt replica (Fig. 13) depending on the properties of the underlying substrate. Smooth Au-coated silicon substrate favors the formation of isolated mounds of Pt replica (Fig. 13a and c). Chemical modification of the Au-coated silicon substrate using a self-assembled monolayer

(SAM) of 1-undecanethiol induced much higher substrate coverage (Fig. 13b and d). Presumably, in comparison to Au, SAM is more energetically neutral to copolymer blocks and does not favor the PFS phase. Surface topography is also found to significantly influence the replication of gyroid Pt over large areas. FTO-glass or Au-coated FTO glass, with the amplitude of surface roughness (*ca.* 50 nm) comparable to the copolymer domain spacing, led to the complete surface coverage and formation of a continuous freestanding array of gyroid Pt replica.

Vignolini et al. [108] demonstrated the creation of a gold optical metamaterial starting from triblock copolymer polyisoprene-*block*-polystyrene-*block*-polyethylene oxide (PI-*b*-PS-*b*-PEO). The polymer adopted the double gyroid morphology with two chemically distinct networks (PI and PEO) in a matrix of polystyrene. The PI network was selectively removed by UV irradiation and subsequent rinsing with ethanol. Then, the polymer template was backfilled with gold by electrochemical deposition and, finally, the remaining template was removed by plasma etching resulting in a single gyroid, nanoscale ordered Au foam. The preparation procedure is schematically depicted in Fig. 14. The single gyroid Au replica was examined under linearly polarized light (Fig. 15). The tested area contained one grain boundary that divided the sample into two domains with the same orientation perpendicular to the substrate surface and the twinning in lateral direction. At the twinning boundary, the angle between [100] directions was found to be about 105° (Fig. 15a). Both domains reflected the identical color when the polarization of incident light was perpendicular to the grain boundary (Fig. 15b). If the polarization of incident light was parallel to the [100] direction of one of the domains (simultaneously, it is almost perpendicular to the [100] direction of the other domain), the largest optical contrast was observed (Fig. 15c). The absorption peak was found to tune sinusoidally between 525 and 630 nm with the polarization direction (Fig. 15e). For the polarization along the [100] direction in the single gyroid Au, the absorption peak appeared at short wavelengths and is red-shifted for polarization in perpendicular direction (Fig. 15d). Additionally,
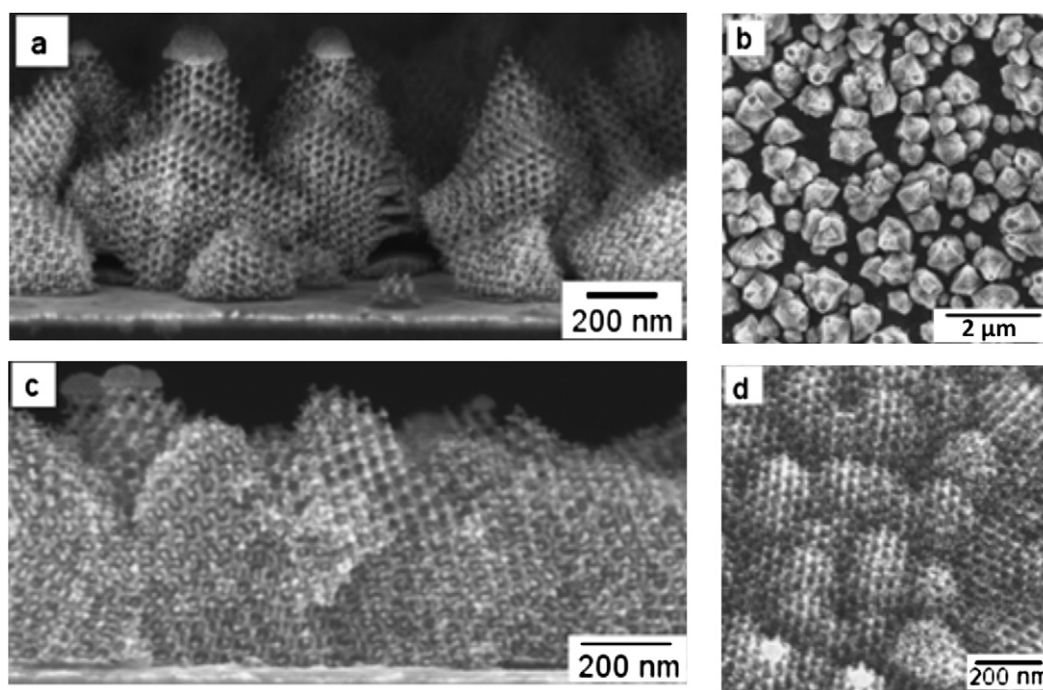
Fig. 13. SEM images in cross-sectional and plan view of two gyroid Pt replicas. a, b) If underlying substrate was Au-coated silicon substrate, isolated mounds of gyroid Pt replica are formed, c, d) If underlying substrate was Au-coated silicon substrate modified with a self-assembled monolayer of 1-undecanethiol, a continuous freestanding array of gyroid Pt replica is formed. Adapted from Ref. [105].
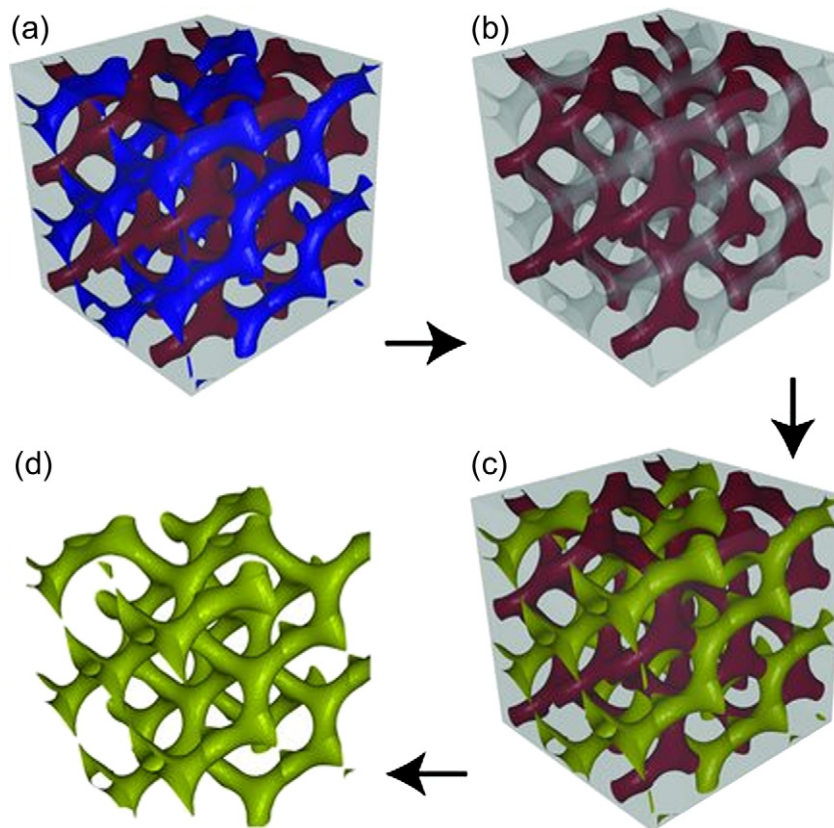
Fig. 14. Schematic representation of sample fabrication: (a) triblock copolymer PI-*b*-PS-*b*-PEO self-assembles into the double gyroid structure with two distinct networks (blue PI and red PEO) in a matrix of PS (grey), (b) the PI block is selectively removed, (c) the polymer template is backfilled with gold (yellow), (d) after the template removal by plasma etching, a single gyroid Au nanofoam is exposed. Reprinted from Ref. [108].

the Au replica exhibits optical chirality. Transmission measurements with circularly polarized light were performed while the sample was rotated around the [110] surface normal. The maximum transmission was observed for two rotation angles in each full turn, *i.e.*, when the optical axis coincides with the gyroid [111] chiral direction.

Warren et al. [109] demonstrated an alternative route towards ordered metal nanofoams via direct self-assembly of block copolymers with ligand-stabilized metal nanoparticles. Block copolymer polyisoprene-*block*-poly(dimethylaminoethyl methacrylate) PI-*b*-PDMAEMA and ligand-stabilized Pt nanoparticles were dissolved in chloroform. The solutions were transferred to Al dishes and heated at 50 °C for approximately 1 h until the solvent completely evaporated. After annealing at 130 °C for 2 days under vacuum, samples adopted the ordered morphology. A cylindrical sample was exposed to rapid pyrolysis and converted to an ordered porous Pt–C composite. Finally, carbon was removed using Ar–O plasma and the Pt nanofoam was exposed. The electrical conductivity of the Pt–C composite was found to be rather high (400 S/cm). This strategy can be extended to different metals and block copolymer morphologies.

Binary mixture of PS-*b*-PI block copolymer and PS homopolymer with an overall PS volume fraction of 0.66 and the double gyroid morphology was prepared by Hashimoto et al. [85] After the selective removal of the PI block by ozonolysis, a gyroid polymer scaffold was electroless nickel plated. Fig. 16 shows the TEM image of the nickel plated sample and the inset highlights 10 nm nickel particles deposited onto the surface of a 25 nm diameter nanochannel, thus leaving a 5 nm diameter empty channel in the middle.

In 2011, our group reported the formation of a freestanding gyroid nickel nanofoam via electroless plating of a block copolymer based template [60]. At the same time, Hsueh et al. [106] published the preparation of gyroid Ni replica starting from PS-*b*-PLLA block copolymers. The unique aspects of our approach will be described next.

7. Supramolecular route to gyroid Ni nanofoams

As mentioned in Section 3, supramolecular complexes of block copolymers containing the P4VP block and amphiphilic PDP molecules have been thoroughly examined in the group of Ikkala and our group. We recently attempted to use supramolecular complexes of triblock copolymer poly(*tert*-butoxystyrene)-*block*-polystyrene-*block*-poly(4-vinylpyridine) PtBOS-*b*-PS-*b*-P4VP and amphiphilic PDP molecules that self-assemble into a core–shell double gyroid morphology as precursors to well-ordered metal nanofoams [59]. The TEM image of the representative core–shell double gyroid PtBOS-*b*-PS-*b*-P4VP(PDP)$_x$ complex (Fig. 17) displays a typical gyroid double-wave pattern. The core channels are emptied by ethanol treatment and subsequently electroless nickel plated. Channels located close to the surface are filled with nickel whilst ones in the middle of the film remain empty as shown in Fig. 18. This seems to be induced by narrow channels (average pore diameter is determined by mercury porosimetry to be 12 nm) and the fast-growing nickel deposit near the free surface that hinders the reagents' diffusion towards the bulk [110].

Subsequently, we evaluated a supramolecular complex PS-*b*-P4VP(PDP) as a precursor to a gyroid nickel nanofoam. Unique to this approach is that the gyroid matrix, or more precisely, part of the matrix, was removed from the complex to render a nanoporous template. Our procedure is schematically summarized in Fig. 19. A
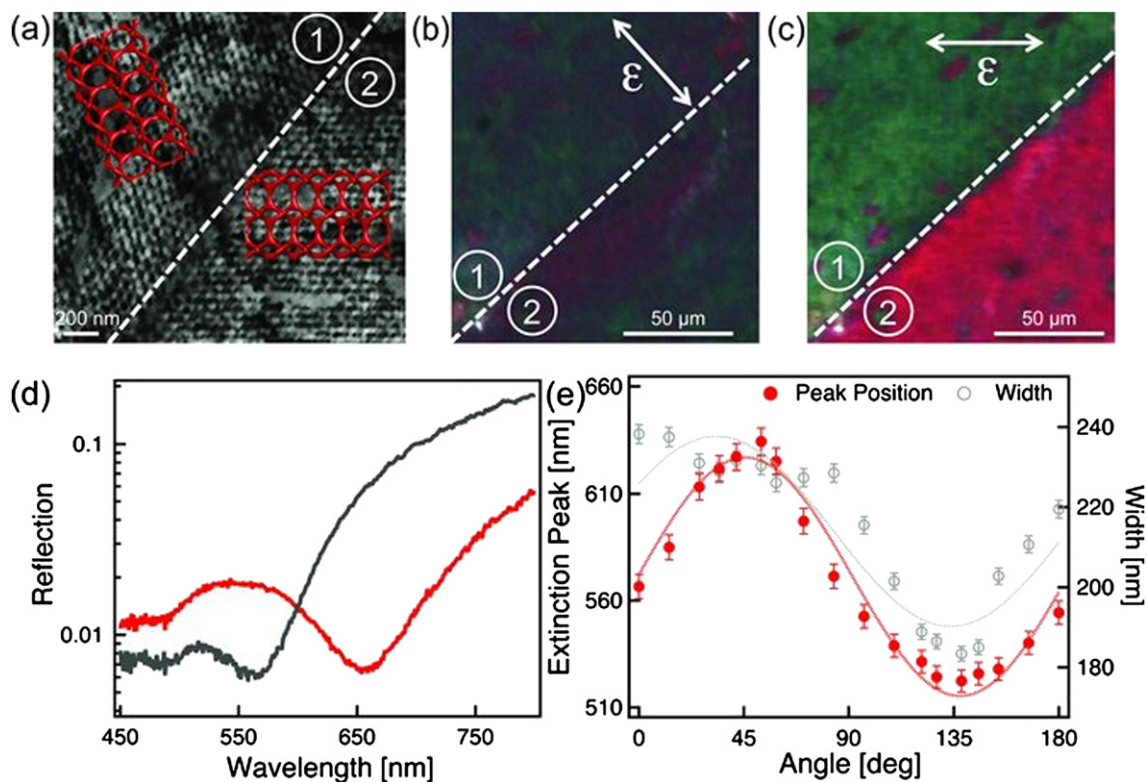
Fig. 15. Linear dichroism of the Au gyroid: (a) SEM image of the examined sample area, (b, c) Optical reflection images obtained with linearly polarized light, perpendicular to the grain boundary (b) or parallel to the [100] gyroid direction of the domain 2 (c), (d) Reflection spectra for area 1 with the polarization perpendicular (red) and parallel (dark grey) to the [100] gyroid direction, (e) Dependence of the extinction (reflectivity) peak position and width on the angle between the [100] gyroid direction and incident light polarization. Reprinted from Ref. [108].
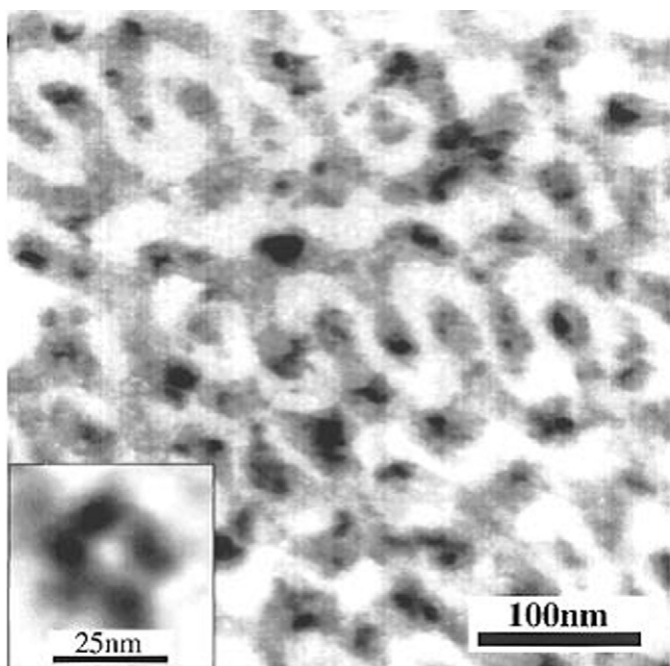

Fig. 16. The TEM image of the electroless nickel plated polymer template with the double gyroid morphology. The inset shows a 25 nm nanochannel coated with 10 nm nickel nanoparticles. Reprinted with permission from Ref. [85]. Copyright 1997 American Chemical Society.
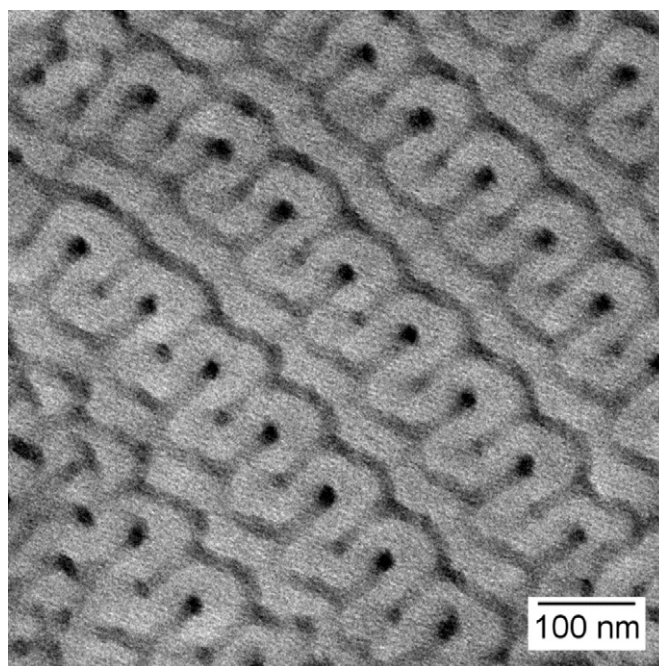
Fig. 17. TEM micrograph of the PtBOS-b-PS-b-P4VP(PDP)$_x$ complex with $x = 0.7$, $f_{PtBOS} = f_{PS} = 0.397$ and $M_{total} = 88\ 300$ g mol^{-1}. P4VP(PDP)$_x$ domains are selectively stained with iodine and appear dark in the image. The double-wave pattern indicates the cross-section through the gyroid [211] plane. Adapted from Ref. [59].
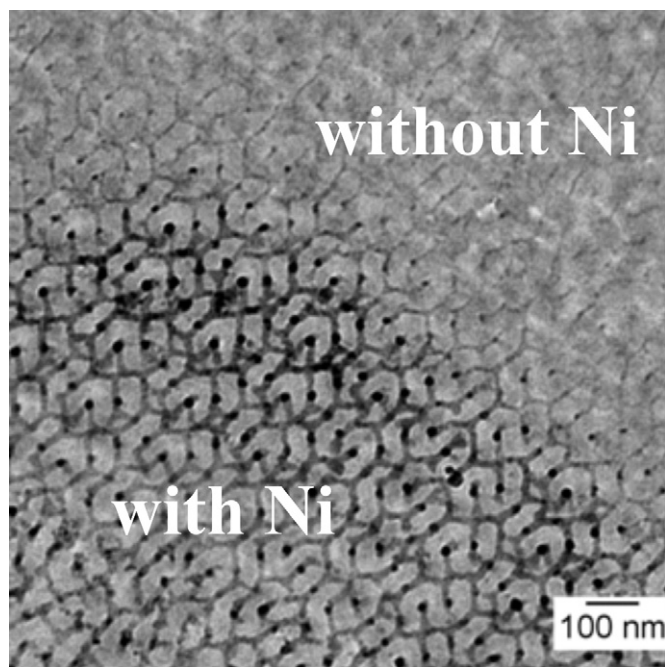
Fig. 18. TEM micrograph of nickel plated gyroid sample derived from the PtBOS-*b*-PS-*b*-P4VP(PDP)$_x$ complex with $x = 0.5$, $f_{P4VP(PDP)} = 0.413$ and $M_{total} = 84\ 800$ g mol^{-1}. Channels located close to the surface are filled with nickel whilst the ones in the middle of the film remain empty. Adapted from Ref. [59].

parent block copolymer PS-*b*-P4VP and hydrogen bonding PDP molecules are dissolved in chloroform and solvent annealed for one week (Fig. 19a). The supramolecular PS-*b*-P4VP(PDP)$_x$ complex (x represents the ratio between the number of PDP molecules and the number of P4VP monomer units) with the double gyroid morphology consisting of PS networks and a P4VP(PDP)$_x$ matrix is obtained (Fig. 19b). Then, the complex is immersed in ethanol, a selective solvent for PDP, which leads to the formation of an open network structure consisting of a PS core and a P4VP corona

(Fig. 19c). Electroless plating is employed to backfill the porous polymer template with nickel (Fig. 19d) and finally, the remaining polymer is removed by pyrolysis and a well-ordered gyroid nickel replica is exposed (Fig. 19e).

Contrary to previously described examples, our porous polymer template PS(core)-P4VP(corona) is obtained by partial removal of the gyroid matrix and represents a double network occupying more than 50 vol%. Removal of the matrix from the gyroid forming conventional diblock copolymers would result in a template occupying only *ca.* 35 vol%, which is not suitable for the formation of a metallic replica with porosity high enough to fulfill the general requirement for metal nanofoams (porosity higher than 50 vol%). Furthermore, the removal of the sacrificial block from conventional block copolymers, such as PS-*b*-PLA or PS-*b*-PEO [111], results in a hydrophobic PS surface that usually requires modification prior to electroless plating in order to achieve the uniform metal deposition [112]. In our approach, the presence of the P4VP hydrophilic corona facilitates the penetration of water-based plating reagents into the porous template and enables successful metal deposition.

The morphology of supramolecular complexes PS-*b*-P4VP(PDP)$_x$ is examined by TEM and SAXS. Fig. 20a and b displays typical gyroid patterns of a representative supramolecular complex: the double-wave and the wagon-wheel patterns that are known to represent projections through the [211] and the [111] plane of the gyroid unit cell, respectively. The PS block domains appear bright whilst the P4VP(PDP)$_x$ block domains appear dark due to iodine staining. Fig. 20c represents the double-wave pattern of a different gyroid sample of which the periodicity is decreased with a factor of 2. SAXS peaks at positions: $\sqrt{6}q^*$, $\sqrt{8}q^*$, $\sqrt{14}q^*$, $\sqrt{22}q^*$, and $\sqrt{50}q^*$ confirm the bicontinuous $Ia\bar{3}d$ morphology of the sample (Fig. 20d).

The complete removal of PDP by subjecting the PS-*b*-P4VP(PDP)$_x$ complex to ethanol is proven by ^{1}H NMR and DSC. After the ethanol treatment, all ^{1}H NMR signals characteristic for PDP are absent and the spectrum of the diblock copolymer is recovered. Additionally, the DSC data imply that the thermal behavior of the ethanol treated sample and that of the diblock copolymer is identical. Textural properties of the representative porous gyroid template are determined by nitrogen adsorption and mercury
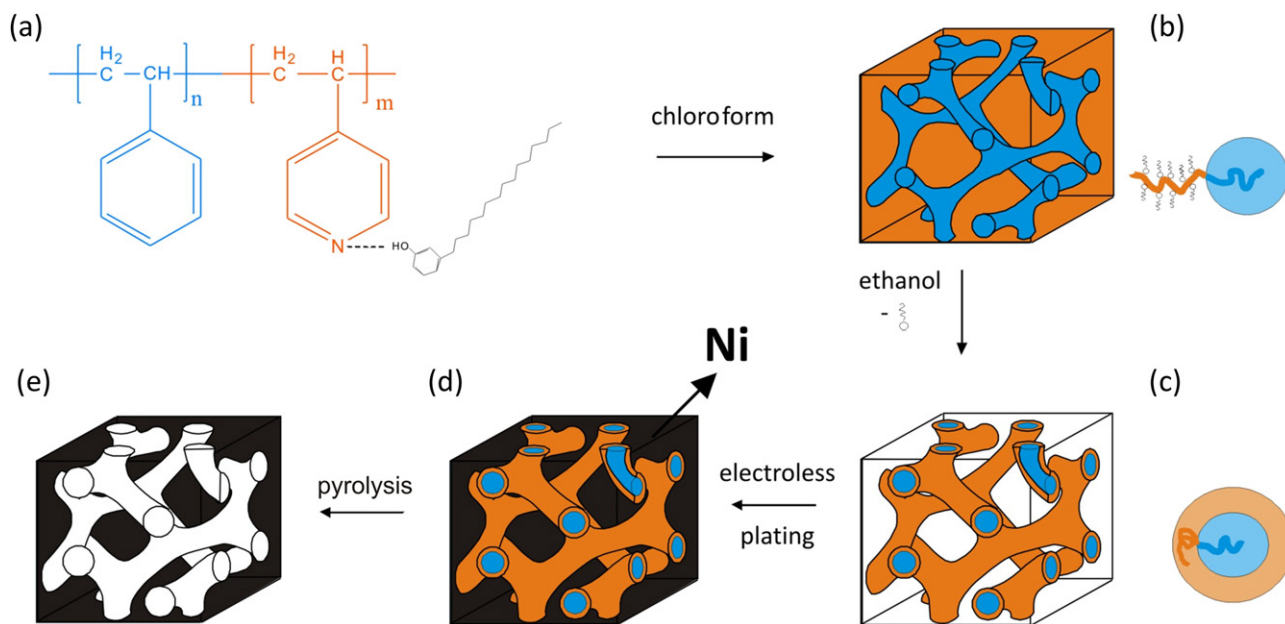
Fig. 19. Schematic representation of sample fabrication via the supramolecular route: (a) PS-*b*-P4VP and PDP are dissolved in chloroform and after one week of solvent annealing, (b) The complex self-assembles into the bicontinuous gyroid morphology. (c) Nanoporous template is obtained by selective PDP dissolution in ethanol. (d) The template is backfilled with nickel by electroless deposition. (e) After pyrolysis, a gyroid nickel nanofoam is exposed. Reprinted with permission from Ref. [60]. Copyright 2011 American Chemical Society.
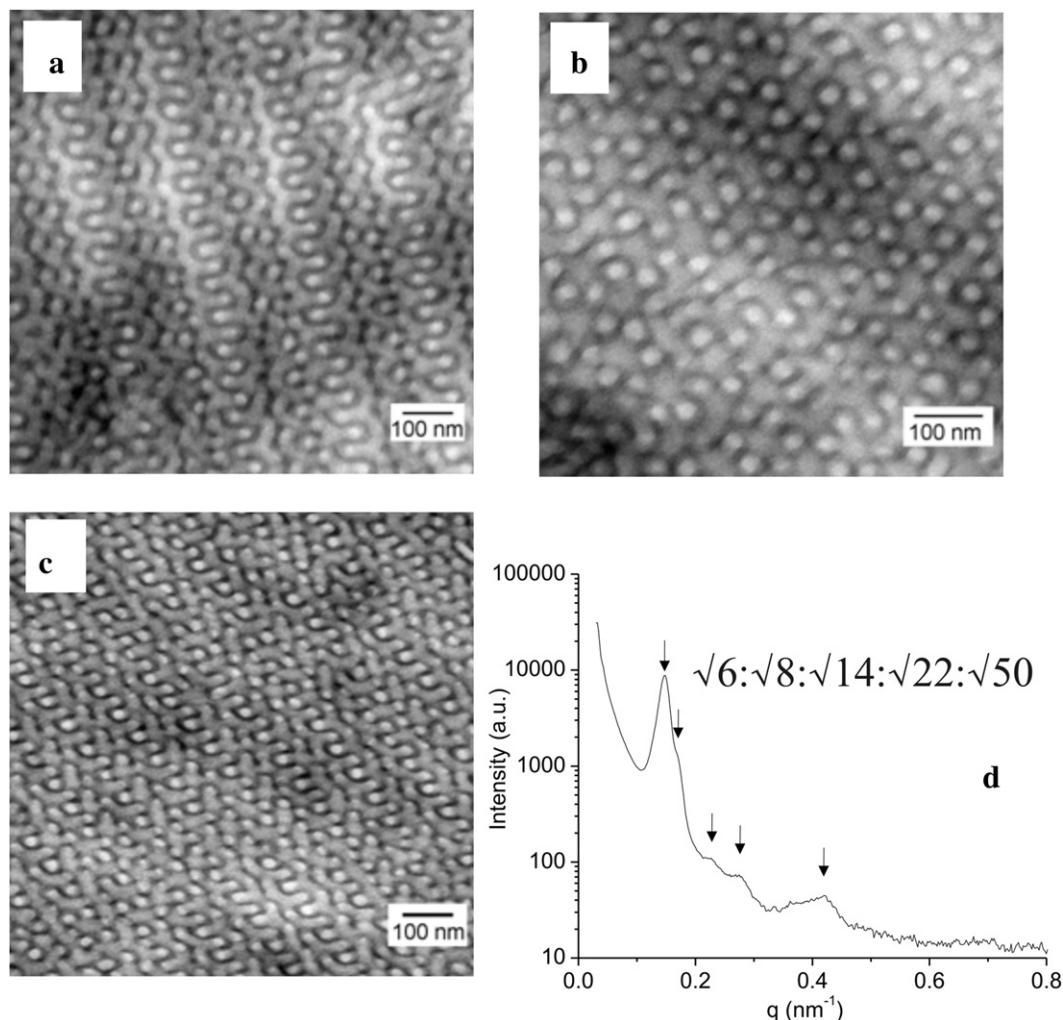
Fig. 20. (a, b) TEM micrographs of the PS-*b*-P4VP(PDP)$_x$ sample with $x = 1.5$, $f_{\text{P4VP(PDP)}} = 0.69$ and $M_{\text{total}} = 135\,000$ g mol^{-1}, representing the double-wave and the wagon-wheel gyroid pattern, respectively. (c, d) TEM micrograph and SAXS pattern of the gyroid PS-*b*-P4VP(PDP)$_x$ sample with $x = 0.8$, $f_{\text{P4VP(PDP)}} = 0.59$ and $M_{\text{total}} = 90\,600$ g mol^{-1}. Reprinted with permission from Ref. [60]. Copyright 2011 American Chemical Society.

porosimetry. The BET specific surface area of 104 m^2 g^{-1} is rather high, the template occupies almost 60 vol%, the average pore diameter is 40 nm, and pore size distribution is very narrow (Fig. 21).
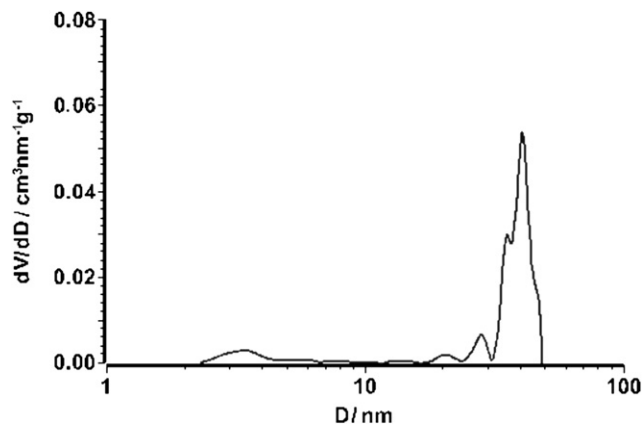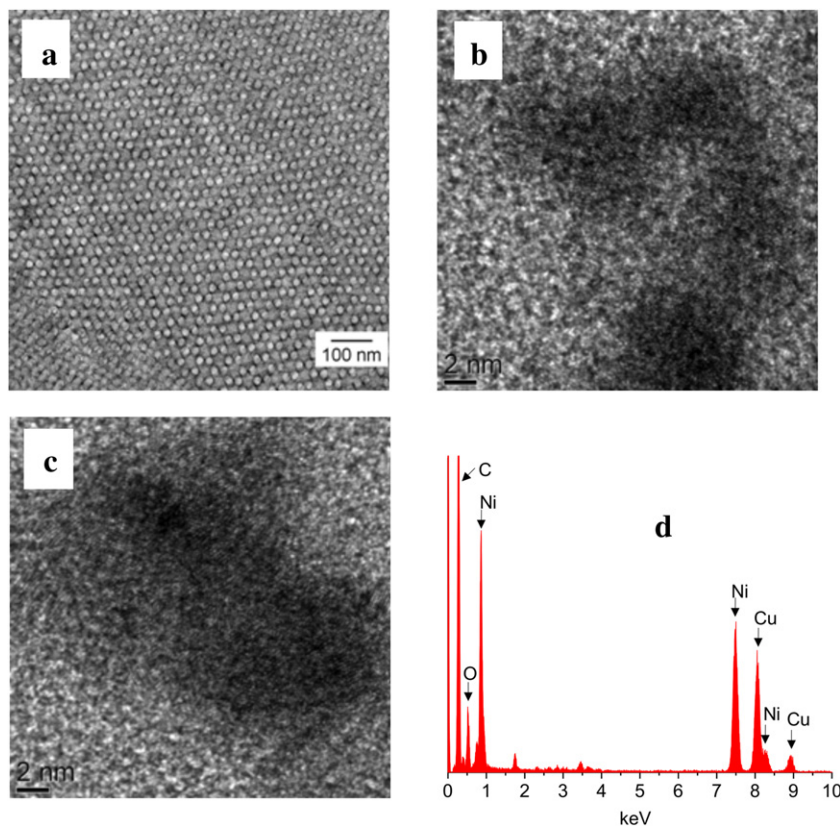

Fig. 21. Pore size distribution of the porous gyroid template derived from PS-*b*-P4VP(PDP)$_x$ complex with $x = 1.0$, $f_{\text{P4VP(PDP)}} = 0.62$ and $M_{\text{total}} = 83\,300$ g mol^{-1}. The graph represents the derivative of the cumulative pore volume *vs* pore diameter. Reprinted with permission from Ref. [60]. Copyright 2011 American Chemical Society.

Prior to electroless plating, the Pd catalyst is deposited onto the gyroid template surface to direct the selective nickel ion reduction. Successively, nickel metal fills the pores of the polymer template. Fig. 22a represents the TEM micrograph of the unstained nickel plated gyroid sample and the contrast in the image originates from metal deposited in the nanochannels. Additionally, the characteristic wagon-wheel pattern confirms the preservation of the double gyroid morphology during the processing steps. HR TEM micrographs (Fig. 22b, c) show relatively large, interconnected Ni crystallites and EDX analysis (Fig. 22d) reveals the chemical composition of the plated sample. As expected, prominent carbon and nickel peaks are observed, together with the oxygen peak that indicates the oxidation of the nickel nanofoam when stored in air.

Finally, the remaining polymer is decomposed by heating isothermally at 350 °C for at least half an hour, leaving the nickel network intact. The exposed nickel replica preserves the inverse gyroid morphology, the shape of the gyroid matrix, as confirmed by SEM (Fig. 23). This shape is the negative of the gyroid networks shape, therefore their surface area is equal and their porosities sum up to 100%. Additionally, this a one-part shape whilst its negative consists of two interpenetrated parts.

In the work that followed, we performed a comprehensive study of the phase behavior of supramolecular complexes PS-*b*-P4VP(PDP)$_x$ in the region of the phase diagram where the gyroid

Fig. 22. (a) TEM image of the unstained nickel plated gyroid polymer template derived from the PS-b-P4VP(PDP)$_x$ complex with $x = 1.0$, $f_{P4VP(PDP)} = 0.62$ and $M_{total} = 83\,300$ g mol^{-1}. The image represents the wagon-wheel gyroid pattern. (b, c) HR TEM images showing relatively large and interconnected Ni crystallites. (d) EDS pattern of the nickel plated sample showing prominent carbon and nickel peaks, together with the oxygen peak that indicates the oxidation of the nickel nanofoam when stored in air. The copper peak originates from the grid used as a support. The nickel plated sample (b, c, d) is derived from the PS-b-P4VP(PDP)$_x$ complex with $x = 0.8$, $f_{P4VP(PDP)} = 0.59$ and $M_{total} = 90\,600$ g mol^{-1}. Reprinted with permission from Ref. [60]. Copyright 2011 American Chemical Society.

morphology with the P4VP(PDP)$_x$ as a majority block was expected [57]. By varying the molar mass and the composition of the starting PS-b-P4VP copolymer and the amount of PDP in the complex, double gyroid templates, and consequently well-ordered gyroid metal nanofoams, with tunable feature sizes and porosities can be obtained. The phase behavior of our supramolecular complexes PS-b-P4VP(PDP)$_x$ on the other side of the phase diagram, *i.e.*, in the region where the gyroid phase with the P4VP(PDP)$_x$ as a minority block was expected, appeared to be quite surprising [58]. Instead of the expected GYR phase, a broad region of the hexagonally perforated layer (HPL) phase is found. The HPL is a metastable phase in conventional block copolymers, but an equilibrium phase in PS-b-P4VP(PDP)$_x$ complexes with the P4VP(PDP)$_x$ as a minority

component. This untypical phase behavior can be explained by the presence of PDP "side chain" molecules in the minority component of the complex, where the HPL morphology reliefs the packing frustrations.

8. Summary and outlook

In this feature article we focus on the preparation and utilization of a new class of materials, metal nanofoams, and discuss the possibility of using block copolymers as a tool for ordered metallic nanostructures. Metal nanofoams have the potential to outperform classical materials in a number of fields: hydrogen storage, production of novel batteries, catalysis, actuating, *etc.* Several
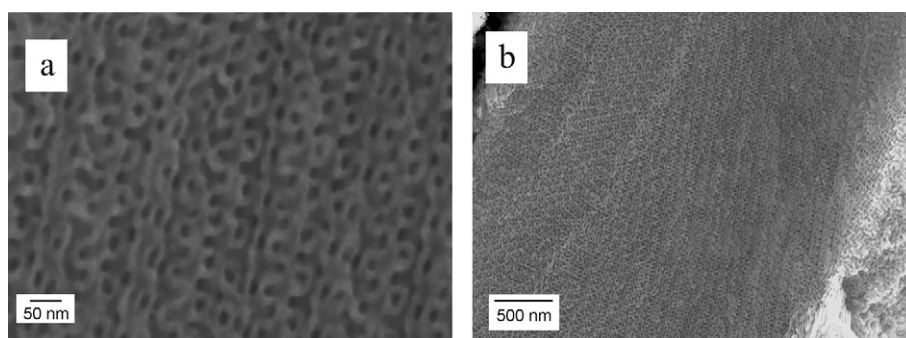
Fig. 23. SEM micrographs of the inverse gyroid nickel replica derived from the PS-b-P4VP(PDP)$_x$ complex with $x = 1.5$, $f_{P4VP(PDP)} = 0.69$ and $M_{total} = 135\,000$ g mol^{-1}. Reprinted with permission from Ref. [60]. Copyright 2011 American Chemical Society.

techniques for their preparation have been developed and most of them result in highly porous, but immensely disordered metal nanofoams. Block copolymers can microphase separate into well-ordered nanostructures from which one of the blocks can be selectively etched. The resulting porous template can be backfilled with metal and subsequently, the remaining polymer can be removed leading to well-ordered metal nanofoams. Even more appealing for this purpose than conventional block copolymers, are supramolecular complexes where side chains hydrogen-bonded to one of the blocks can be removed by simple dissolution. Additionally, the morphology of these complexes can be easily tailored by alteration of the amount of added side chains. The bicontinuous gyroid morphology appears as the most suitable nanostructure to provide the interconnected, structurally isotropic metal nanofoams. Pt, Au and Ni gyroid replicas have already been reported in the literature and their application in different fields evaluated.

In the future, we expect metal nanofoam characteristics to be improved and adjusted to meet the requirements for desired applications. For instance, their structure can be tailored by employing alternative block copolymer phases as precursors, such as the orthorhombic *Fddd* network or plumber's nightmare phase. Additionally, their chemical composition can be varied and alternative metals, such as Ag, Cu, Co, *etc.*, can be deposited in the polymer template channels, leading to new ordered metal nanofoams. Furthermore, block copolymer template-directed synthesis can be combined with dealloying; from the alloy deposited in block copolymer template channels, a less noble metal can be removed, leading to a hierarchically porous ordered metal nanofoam. In addition, block copolymer templates can be oriented by, for instance, electric fields [113] or large amplitude oscillatory shearing [114,115]. Oriented block copolymer templates will lead to metal nanofoams with improved ordering which might have superior properties, as actuators, for example, in comparison to the existing metal nanofoams. The synthetic routes towards well-ordered metal nanofoams and their application potential are still poorly examined and we expect further investigation and exciting discoveries to emerge.

References

[1] Mahtab R, Rogers JP, Murphy CJ. J Am Chem Soc 1995;117(35):9099–100.
[2] Weissleder R, Elizondo G, Wittenburg J, Rabito C, Bengele H, Josephson L. Radiology 1990;175:489–93.
[3] de la Isla A, Brostow W, Bujard B, Estevez M, Rodriguez JR, Vargas S, et al. Mat Resr Innovat 2003;7:110–4.
[4] Salata OV. J Nanobiotechnol 2004;2:3–8.
[5] Roy I, Ohulchanskyy TY, Pudavar HE, Bergey EJ, Oseroff AR, Morgan J, et al. J Am Chem Soc 2003;125(26):7860–5.
[6] Duncan TV. J Colloid Interface Sci 2011;363:1–24.
[7] Cuenya BR. Thin Solid Films 2010;518:3127–50.
[8] Yamauchi M, Kobayashi H, Kitagawa H. ChemPhysChem 2009;10(15):2566–76.
[9] Pasquini L, Brighi M, Montone A, Antisari MV, Dam B, Palmisano V, et al. IOP Conf Ser Mater Sci Eng 2012;38:12001–8.
[10] Reiss G, Hutten A. Nat Mater 2005;4:725–6.
[11] Xia Y, Yang P, Sun Y, Wu Y, Mayers B, Gates B, et al. Adv Mater 2003;15(5):353–89.
[12] Yuan J, Müller AHE. Polymer 2010;51(18):4015–36.
[13] Park S, Kim B, Cirpan A, Russell T. Small 2009;5(11):1343–8.
[14] Smith D. Thin film deposition: principles and practice. New York: McGraw-Hill; 1995.
[15] George SM. Chem Rev 2010;110:111–31.
[16] Knoll W, Advincula RC. Functional polymer films. Wiley-VCH; 2011.
[17] Zhou W, Wang ZL. Three-dimensional nanoarchitectures. New York: Springer; 2011.
[18] Tappan BC, Steiner SA, Luther EP. Angew Chem Int Ed 2010;49(27):4544–65.
[19] Berube V, Radtke G, Dresselhaus M, Chen G. Int J Energy Res 2007;31(6–7):637–63.
[20] Sakintuna B, Lamari-Darkrim F, Hirscher M. Int J Hydrogen Energy 2007;32(9):1121–40.
[21] Berube V, Chen G, Dresselhaus MS. Int J Hydrogen Energy 2008;33(15):4122–31.
[22] Rolison DR, Long JW, Lytle JC, Fischer AE, Rhodes CP, McEvoy TM, et al. Chem Soc Rev 2009;38(1):226–52.
[23] Gleiter H, Weissmüller J, Wollersheim O, Würschum R. Acta Mater 2001;49(4):737–45.
[24] Jin H-J, Weissmüller J. Adv Eng Mater 2010;12(8):714–23.
[25] Kramer D, Viswanath RN, Weissmüller J. Nano Lett 2004;4(5):793–6.
[26] Bobyn JD, Stackpool GJ, Hacking SA, Tanzer M, Krygier JJ. J Bone Jt Surg Br 1999;81:907–14.
[27] Willie BM, Yang X, Kelly NH, Merkow J, Gagne S, Ware R, et al. J Biomed Mater Res B Appl Biomater 2010;92:479–88.
[28] Erlebacher J, Aziz MJ, Karma A, Dimitrov N, Sieradzki K. Nature 2001;410:450–3.
[29] Detsi E, van de Schootbrugge M, Punzhin S, Onck PR, De Hosson JTM. Scripta Mater 2011;64(4):319–22.
[30] Nyce GW, Hayes JR, Hamza AV, Satcher JH. Chem Mater 2007;19(3):344–6.
[31] Gacoin T, Lahlil K, Larregaray P, Boilot JP. J Phys Chem B 2001;105(42):10228–35.
[32] Leventis N, Chandrasekaran N, Sotiriou-Leventis C, Mumtaz A. J Mater Chem 2009;19(1):63–5.
[33] Leventis N, Chandrasekaran N, Sadekar AG, Sotiriou-Leventis C, Lu H. J Am Chem Soc 2009;131(13):4576–7.
[34] Tappan BC, Huynh MH, Hiskey MA, Chavez DE, Luther EP, Mang JT, et al. J Am Chem Soc 2006;128(20):6589–94.
[35] Ashby MF, Evans AG, Fleck NA, Gibson LJ, Hutchinson JW, Wadley HG. Metal foams: a design guide. Oxford, UK: Butterworth-Heinemann; 2000.
[36] Tekoglu C. Size effects in cellular solids. University of Groningen; 2007.
[37] Amsterdam E. Structural performance and failure analysis of aluminium foams. University of Groningen; 2008.
[38] Hamley IW. The physics of block copolymers. Oxford: Oxford University Press; 1998.
[39] Bates FS, Fredrickson GH. Annu Rev Phys Chem 1990;41:525–7.
[40] Abetz V, Simon P. Phase behaviour and morphologies of block copolymers. Advances in polymer science. Berlin/Heidelberg: Springer; 2005.
[41] Abetz V, Boschetti-de-Fierro A. Block copolymers in the condensed state. In: Matyjaszewski K, Möller M, editors. Polymer science: a comprehensive reference, vol. 7. Amsterdam: Elsevier BV; 2012. p. 3–44.
[42] Matsen MW. J Phys Condens Matter 2002;14:R21–47.
[43] Matsen MW, Schick M. Phys Rev Lett 1994;72(16):2660–3.
[44] Matsen MW, Bates FS. Macromolecules 1996;29(4):1091–8.
[45] Khandpur AK, Foerster S, Bates FS, Hamley IW, Ryan AJ, Bras W, et al. Macromolecules 1995;28(26):8796–806.
[46] Bates FS, Fredrickson GH. Phys Today 1999;52:32–8.
[47] Epps TH, Cochran EW, Bailey TS, Waletzko RS, Hardy CM, Bates FS. Macromolecules 2004;37(22):8325–41.
[48] Tyler CA, Qin J, Bates FS, Morse DC. Macromolecules 2007;40(13):4654–68.
[49] Gobius du Sart G, Vukovic I, Alberda van Ekenstein G, Polushkin E, Loos K, ten Brinke G. Macromolecules 2010;43(6):2970–80.
[50] Faber M, Voet VSD, ten Brinke G, Loos K. Soft Matter 2012;8(16):4479–85.
[51] Matsushita Y. Macromolecules 2007;40(4):771–6.
[52] Ruokolainen J, ten Brinke G, Ikkala O. Adv Mater 1999;11(9):777–80.
[53] Ruokolainen J, Saariaho M, Ikkala O, ten Brinke G, Thomas EL, Torkkeli M, et al. Macromolecules 1999;32(4):1152–8.
[54] Mäki-Ontto R, de Moel K, de Odorico W, Ruokolainen J, Stamm M, ten Brinke G, et al. Adv Mater 2001;13:117–21.
[55] Ikkala O, ten Brinke G. Science 2002;295:2407–9.
[56] Valkama S, Ruotsalainen T, Nykänen A, Laiho A, Kosonen H, ten Brinke G, et al. Macromolecules 2006;39(26):9327–36.
[57] Vukovic I, Voortman TP, Merino DH, Portale G, Hiekkataipale P, Ruokolainen J, et al. Macromolecules 2012;45(8):3503–12.
[58] Vukovic I, ten Brinke G, Loos K. Macromolecules 2012;45(23):9409–18.
[59] Gobius du Sart G, Vukovic I, Vukovic Z, Polushkin E, Hiekkataipale P, Ruokolainen J, et al. Macromol Rapid Commun 2011;32(4):366–70.
[60] Vukovic I, Punzhin S, Vukovic Z, Onck P, De Hosson JTM, ten Brinke G, et al. ACS Nano 2011;5(8):6339–48.
[61] Luzzati V, Spegt P. Nature 1967;215:701–2.
[62] Schoen AH. NASA technical note, TN D-5541 1970.
[63] Meuler AJ, Hillmyer MA, Bates FS. Macromolecules 2009;42:7221–50.
[64] Aggarwal SL. Polymer 1976;17:938–56.
[65] Alward DB, Kinning DJ, Thomas EL, Fetters LJ. Macromolecules 1986;19:215–24.
[66] Thomas EL, Alward DB, Kinning DJ, Martin DC, Handlin DL, Fetters LJ. Macromolecules 1986;19:2197–202.
[67] Anderson DM, Thomas EL. Macromolecules 1988;21(11):3221–30.
[68] Likhtman AE, Semenov AN. Macromolecules 1994;27(11):3103–6.
[69] Olmsted PD, Milner ST. Phys Rev Lett 1994;72(6):936–9.
[70] Olmsted PD, Milner ST. Phys Rev Lett 1995;74(5):829.
[71] Hajduk DA, Harper PE, Gruner SM, Honeker CC, Kim G, Thomas EL, et al. Macromolecules 1994;27(15):4063–75.
[72] Schulz MF, Bates FS, Almdal K, Mortensen K. Phys Rev Lett 1994;73(1):86–9.
[73] Goldacker T, Abetz V. Macromolecules 1999;32(15):5165–7.
[74] Shefelbine TA, Vigild ME, Matsen MW, Hajduk DA, Hillmyer MA, Cussler EL, et al. J Am Chem Soc 1999;121(37):8457–65.
[75] Martín-Moreno L, García-Vidal FJ, Somoza AM. Phys Rev Lett 1999;83(1):73–5.
[76] Urbas AM, Maldovan M, DeRege P, Thomas EL. Adv Mater 2002;14(24):1850–3.
[77] Michielsen K, Kole JS. Phys Rev B 2003;68(11):115107.

[78] Thurn-Albrecht T, Schotter J, Kästle GA, Emley N, Shibauchi T, Krusin-Elbaum L, et al. Science 2000;290(5499):2126–9.

[79] Sidorenko A, Tokarev I, Minko S, Stamm M. J Am Chem Soc 2003;125(40):12211–6.

[80] Olayo-Valles R, Guo S, Lund MS, Leighton C, Hillmyer MA. Macromolecules 2005;38(24):10101–8.

[81] Saranathan V, Osuji CO, Mochrie SGJ, Noh H, Narayanan S, Sandy A, et al. PNAS 2010;107:11676–81.

[82] Suzuki J, Seki M, Matsushita Y. J Chem Phys 2000;112(10):4862–8.

[83] Ghoshal T, Maity T, Godsell JF, Roy S, Morris MA. Adv Mater 2012;24(18):2390–7.

[84] Mansky P, Harrison CK, Chaikin PM, Register RA, Yao N. Appl Phys Lett 1996;68(18):2586–8.

[85] Hashimoto T, Tsutsumi K, Funaki Y. Langmuir 1997;13(26):6869–72.

[86] Chen S-Y, Huang Y, Tsiang RC-C. J Polym Sci A Polym Chem 2008;46(6):1964–73.

[87] Thurn-Albrecht T, Steiner R, DeRouchey J, Stafford CM, Huang E, Bal M, et al. Adv Mater 2000;12(11):787–91.

[88] Joo W, Yang SY, Kim JK, Jinnai H. Langmuir 2008;24(21):12612–7.

[89] Zalusky AS, Olayo-Valles R, Taylor CJ, Hillmyer MA. J Am Chem Soc 2001;123(7):1519–20.

[90] Zalusky AS, Olayo-Valles R, Wolf JH, Hillmyer MA. J Am Chem Soc 2002;124(43):12761–73.

[91] Crossland EJW, Kamperman M, Nedelcu M, Ducati C, Wiesner U, Smilgies DM, et al. Nano Lett 2008;9(8):2807–12.

[92] Uehara H, Kakiage M, Sekiya M, Sakuma D, Yamonobe T, Takano N, et al. ACS Nano 2009;3(4):924–32.

[93] Voet VSD, Tichelaar M, Tanase S, Mittelmeijer-Hazeleger MC, ten Brinke G, Loos K. Nanoscale 2013;5(1):184–92.

[94] Park M, Harrison C, Chaikin PM, Register RA, Adamson DH. Science 1997;276(5317):1401–4.

[95] Cheng JY, Ross CA, Thomas EL, Smith HI, Vancso GJ. Appl Phys Lett 2002;81(19):3657–9.

[96] Farrell RA, Petkov N, Shaw MT, Djara V, Holmes JD, Morris MA. Macromolecules 2010;43(20):8651–5.

[97] Voet VSD, Pick TE, Park S-M, Moritz M, Hammack AT, Urban JJ, et al. J Am Chem Soc 2011;133(9):2812–5.

[98] Brinker CJ, Scherer JW. Sol–gel science: the physics and chemistry of sol–gel processing. Boston: Academic Press; 1990.

[99] Hsueh H-Y, Chen H-Y, She M-S, Chen C-K, Ho R-M, Gwo S, et al. Nano Lett 2010;10(12):4994–5000.

[100] Hsueh H-Y, Ho R-M. Langmuir 2012;28(22):8518–29.

[101] Riedel W. Electroless nickel plating. Metals Park: Finishing Publications; 1991.

[102] Mallory GO, Hajdu JB. Electroless plating: Fundamentals and applications. American Electroplaters and Surface Finishers Society; 1992.

[103] Djokić SS. In: Conway BE, White RE, editors. Electroless deposition of metals and alloys, vol. 35. US: Springer; 2002. p. 51–133.

[104] Djokić SS, Cavallotti PL. Electroless deposition: theory and applications, vol. 48. New York: Springer; 2010251–89.

[105] Crossland EJW, Ludwigs S, Hillmyer MA, Steiner U. Soft Matter 2010;6(3):670–6.

[106] Hsueh HY, Huang YC, Ho RM, Lai CH, Makida T, Hasegawa H. Adv Mater 2011;23(27):3041–6.

[107] Hakamada M, Mabuchi M. J Mater Res 2009;24(2):301–4.

[108] Vignolini S, Yufa NA, Cunha PS, Guldin S, Rushkin I, Stefik M, et al. Adv Mater 2012;24(10):OP23–7.

[109] Warren SC, Messina LC, Slaughter LS, Kamperman M, Zhou Q, Gruner SM, et al. Science 2008;320(5884):1748–52.

[110] Boontongkong Y, Cohen RE, Rubner MF. Chem Mater 2000;12(6):1628–33.

[111] Mao H, Hillmyer MA. Soft Matter 2006;2(1):57–9.

[112] Kobayashi Y, Tadaki Y, Nagao D, Konno M. J Phys Conf Ser 2007;61:582–6.

[113] Liedel C, Pester CW, Ruppel M, Urban VS, Böker A. Macromol Chem Phys 2012;213(3):259–69.

[114] Faber M, Hofman AH, Polushkin E, van Ekenstein GA, Seitsonen J, Ruokolainen J, et al. Macromolecules 2013;46(2):500–17.

[115] Vukovic I. Block copolymer template-directed synthesis of well-ordered metallic nanostructures. University of Groningen; 2013.

[116] http://www.shapeways.com/shops/virtox.

Ivana Vukovic is pursuing her Ph.D. in the Department of Polymer Chemistry at the University of Groningen, The Netherlands, under the supervision of Prof. Gerrit ten Brinke and Prof. Katja Loos. She received her M.S. in Chemical Engineering from the University of Belgrade, Serbia, in 2009. Her current research interest focuses on the design and the application of self-assembled block copolymers and block copolymer-based supramolecular complexes and on well-defined inorganic nanostructures obtained from them. She will continue her career as a researcher in Shell Technology Center in Amsterdam.

Gerrit ten Brinke obtained his PhD in Statistical Physics from the University of Groningen, The Netherlands. He spent two years as a postdoctoral fellow at the University of Massachusetts at Amherst. In 1985 he became Associate Professor in the Polymer Department of the University of Groningen and in 1996 Professor. During 1994–1999 he was also part time Professor at the Helsinki University of Technology working closely together with Olli Ikkala. His research interests are self-assembly in complex polymer systems.

Katja Loos is Professor at the Department of Polymer Chemistry of the University of Groningen, The Netherlands. Her main research interests are currently the different aspects of enzymatic polymerizations and modifications of polymers, biocatalytic synthesis of novel monomers, polysaccharides, the interaction of proteins with specialized surfaces, living polymerization techniques and block copolymer self-assemblies. She specialized in Organic Chemistry and Polymer Chemistry during her university studies at the Johannes Gutenberg Universität in Mainz, Germany & the University of Massachusetts, Amherst, USA and moved into the field of Enzymatic Polymerizations during her doctoral research at the University of Bayreuth, Germany & the Universidade Federal do Rio Grande do Sul, PortoAlegre, Brasil. After a research stay as a Humboldt Fellow at the Polytechnic University in Brooklyn, NY, USA she started an independent research group at the Zernike Institute for Advanced Materials at the University of Groningen. She is currently an VIDI laureate of the Netherlands Organisation for Scientific Research (NWO) and a Fellow of the Dutch Polymer Institute (DPI).